



Research Article

Synthesis and Characterization of Azo-based Compounds as Energy Storage Materials

Pramod Kumar Yadav

Dept. of Chemistry, TU, Thakur Ram Multiple Campus, Birgunj, Nepal

Article Information

Received: 15 November 2023.

Revised version received: 23 December 2023.

Accepted: 25 December 2023.

Published: 29 December 2023.

Cite this article as:

P.K. Yadav (2023) *Int. J. Appl. Sci. Biotechnol.* Vol 11(4): 217-221. DOI: [10.3126/ijasbt.v11i4.61164](https://doi.org/10.3126/ijasbt.v11i4.61164)

*Corresponding author

Pramod Kumar Yadav,

Dept. of Chemistry, TU, Thakur Ram Multiple Campus,
Birgunj, Nepal

Email: pramodkryadav1155@gmail.com

Peer reviewed under authority of IJASBT

©2023 International Journal of Applied Sciences and
Biotechnology

OPEN ACCESS



This is an open access article & it is licensed under a Creative
Commons Attribution Non-Commercial 4.0 International
(<https://creativecommons.org/licenses/by-nc/4.0/>)

Keywords: Azo-compounds, metal-organic frameworks, rechargeable batteries, redox flow batteries, lithium-ion batteries, capacity, capability, high-energy-density

Abstract

Two redox active azo-based materials have been synthesized and characterized by elemental analysis (C, H, N), IR, NMR (^1H & ^{13}C) and single crystal X-ray diffraction analysis. Both the azo-based materials, the ligand **1** and its MOF **2** exhibit good electrochemical performances but the capacity of MOF **2** is higher than the ligand **1**.

Introduction

Recently, the attention of the scientific community has been focused on the high-performance energy storage systems such as rechargeable and redox flow batteries in the view of the ongoing development of electrical devices and increasing demand for sustainable energy. The high-energy-density rechargeable lithium-ion batteries are widely used in portable electronic devices (Hu *et al.*, 2013) and generate power by the redox reactions of electrode-active materials (Lyu *et al.*, 2021). On the other hand, the redox flow

batteries generate power by the redox reactions of their electrolytes (Yan & Wang, 2018).

Aromatic azo-compounds have been used as active materials with reversible redox activity because of the two electron redox reaction based on N=N/N-N and π -conjugation of N=N group to aromatic groups. Furthermore, they have been used as anode or cathode active materials of rechargeable batteries, and organic or aqueous anolyte of redox flow batteries because of their high capacity and high

capability due to electrochemical properties of the N=N group (Fu *et al.*, 2009).

Azo compounds exhibit poor cyclic performance because of their high solubility in organic electrolytes. This performance can be improved by introduction of carboxylate groups (Luo *et al.*, 2018).

Metal-organic frameworks (MOFs) are a class of compounds consisting of metal clusters coordinated to organic ligands to form crystalline porous materials with specific surface area. MOFs with redox activity are of current interest as electrode materials for Li-ion batteries (LIBs) to enhance the lithium storage performance. Redox active MOFs as electrode materials for LIBs are quite rare (Li *et al.*, 2017). It is of great importance to choose redox active metal sites and an appropriate ligand for synthesis of porous MOFs that could be used directly to prepare electrodes for LIBs. The ligand that has been used in this paper, azobenzene-4,4'-dicarboxylic acid (H₂ABDA), is a novel azo-benzenedicarboxylic acid with open negatively charge O sites. It could undergo redox activity through the open negatively charged O sites, which might enhance the battery performances (Wu *et al.*, 2017).

Based on the above-mentioned facts, an azo-based MOF from Zn(1,10-phen). (NO₃)₂.H₂O metal salt with the azobenzenedicarboxylic acid was synthesized. The ligand and the MOF were used to prepare electrodes for LIBs to study their electrochemical performances.

Experimental section

All reagents and solvents were commercially available and used as received. The carbon, nitrogen, and hydrogen contents of the compounds were determined by Carbo-Erba elemental analyzer 1108. The infrared spectra of the compounds were recorded on a Varian 3100 FT-IR spectrometer (4000–400cm⁻¹) using KBr disks.

¹H and ¹³C NMR spectra of compounds were recorded using JEOL AL 300 MHz spectrometer. The starting compound azobenzene-4, 4'-dicarboxylic acid **1** and azobenzene-4, 4'-dicarbonyl chloride **2** were synthesized following reported methods used (Ghosh *et al.*, 2008).

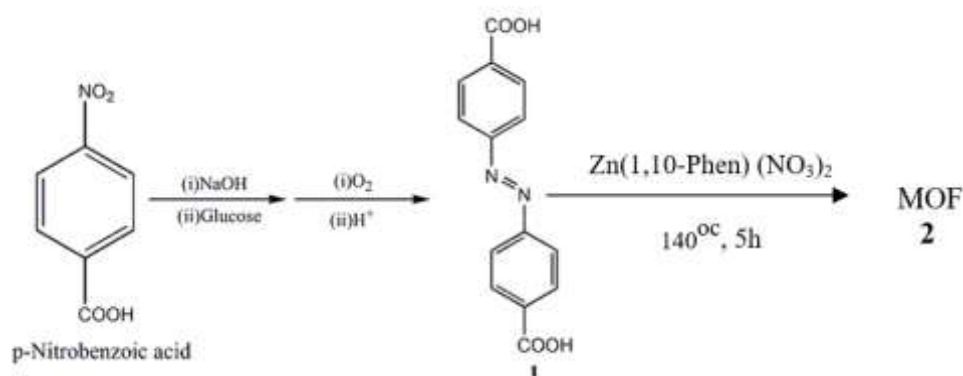
Synthesis of H₂ABDA **1**

The ligand azobenzene-4, 4'-dicarboxylic acid **1** was synthesized following reported method used (Ghosh *et al.*, 2008). For the synthesis of H₂ABDA, *p*-Nitrobenzoic acid (15 g, 67.5 mmol) and NaOH (50 g, 1.25 mmol) were mixed in water (225 mL), and the solution was heated on a water bath until the solid dissolved; hot aqueous glucose (100 g in 150 mL of water) was then added slowly into the above mixture at 50 °C whereupon a yellow precipitate was obtained, which immediately changed to a brown solution upon further addition of glucose. This reaction was highly exothermic. Then, a stream of air was passed into the mixture for 3 h and a light brown precipitate was obtained. This was filtered, dissolved in water, and acidified with acetic acid (25 mL) whereupon a light pink precipitate was obtained. This was filtered, washed with plenty of water (300 mL), and dried in a desiccator to obtain H₂ADA as a brownish orange powder. The analytical data of the compound **1** are as follows: Brownish orange solid, yield 80%, m.p. 335 °C, IR (KBr) ν cm⁻¹: 1683(C=O), 1600(N=N); ¹H NMR(CDCl₃) δ : 13.3 (2H, s, COOH), 8.16 (4H, *J*= 8.4 Hz, d, Ar), 8.01 (4H, *J*= 8.1 Hz, d, Ar); ¹³C NMR (CDCl₃) δ : 166(COOH), 154(Ar), 133(Ar), 130(Ar), 122(Ar); analysis for C₁₄H₁₀N₂O₄: 58.53 (58.34), 4.06 (4.53), 11.38 (11.04).

Synthesis of MOF **2**

The MOF **2** was synthesized by a reported method (Guo *et al.*). In a typical synthetic procedure, Zn^{II} (1,10-phen)(NO₃)₂.H₂O (0.405 g, 1mmol) was added to the solution of azobenzene-4,4'-dicarboxylic acid (0.135g, 0.5mmol) dissolved in DMF/DMSO (6 ml). The mixture was heated at 140°C for 5h to give red crystals of **2**. The complex thus isolated was found to be insoluble in water and common organic solvents. Yield: ~75%. Anal. Calc. for C₅₂H₃₂N₈O₈Zn₂ **2**: C, 60.78; H, 3.14; N, 10.90%. Found: C,60.70; H,3.70; N,11.20%. IR (KBr, cm⁻¹): 3418(w), 3062(m), 1680(s), 1601(s),1552(s), 1427(s), 1389(vs), 1220(m), 1101(m), 1009(m), 858(s), 794(s), 722(s), 641(m), 504(m), 420(m).

Scheme 1: Synthetic strategy of **1** & **2**



Single crystal X-ray analysis of 2: For X-ray Crystallographic Study, the X-ray diffraction data were collected by mounting a single crystal of the sample on glass fibers. Oxford diffraction XCALIBUR-EOS diffractometer was used for the determination of cell parameters and intensity data collection at room temperature. Monochromating Mo K α radiation ($\lambda = 0.71073 \text{ \AA}$) was used for the measurements. The crystal structures were solved by direct methods using SHELXS-97 Program (Sheldrick, 1997) and were refined by full matrix least-squares SHELXL-97 (Sheldrick, 1990). Drawings were carried out using MERCURY (Bruno *et al.*, 2002) and special computations were carried out with PLATON (Spek, 2003).

Electrochemical Measurements

measurements were carried out using coin-type half cells ($d = 1.1 \text{ cm}$), which were assembled in a box filled with argon. The working electrode was prepared by grinding 60 wt% MOF, 30 wt% conductive material (carbon black, SP) and 10 wt% binder (polyvinylidene difluoride, PVDF) in N-methyl-2-pyrrolidone (NMP) solvent to form a homogeneous slurry, and then coating onto copper foil with a thickness of 200 nm and dried at 100 $^{\circ}\text{C}$ for 12 hours under vacuum. Lithium foil and a polypropylene film were used as the counter electrode and the separator, respectively. The electrolyte was 1 M LiPF $_6$ in a mixture of ethylene carbonate and dimethyl carbonate (Zhou *et al.*, 2019).

Results and Discussions

The infrared spectra of **1** shows peak at 1683 cm^{-1} due to C=O stretching vibration. The peak at 1600 cm^{-1} correspond to N=N stretching vibrations of **1**. ^1H NMR spectra exhibit peak at $\delta = 13.3$ due to COOH proton of **1**. ^{13}C NMR spectra of **1** exhibit peaks at $\delta = 166 \text{ ppm}$ due to C=O carbon. The characteristic band of carboxylic acid group observed at 1681 cm^{-1} in the spectrum of free ligand **1**, was absent in the spectrum of its complex **2**. It supported that deprotonated ligand had coordinated with metal ion in the complex **2**.

The peaks observed at 1680 cm^{-1} in the infrared spectra of complex **2** was assigned to $\nu_{\text{asym}}(-\text{COO}^-)$ vibration, whereas $\nu_{\text{sym}}(-\text{COO}^-)$ vibration was observed at 1601 cm^{-1} .

Crystallographic data and refinement details for the structural analyses of **2** are summarized in Table 1. Selected bond lengths and bond angles with their estimated standard deviations are presented in Table 2, while selected parameters for weak interactions are listed in Table 3. Crystallographic data for the compound **2** has been deposited with the Cambridge data centre. The deposition number is CCDC 850421 (Yadav *et al.*, 2012).

Table 1: Crystal data and refinement detail for **2**

Parameters	2
formula	C $_{52}$ H $_{32}$ N $_8$ O $_8$ Zn $_2$
M	1027.60
Crystal system	Monoclinic
Temperature/K	293
Space group	C 2/c
a(\AA)	29.2153(11)
b(\AA)	18.7144(6)
c(\AA)	20.3431(7)
α (deg)	90
β (deg)	107.516(4)
γ (deg)	90
V(\AA^3)	107.516(4)
Z	8
D $_c$ (mg m^{-3})	1.287
Absorption coefficient	0.962 mm^{-1}
F(000)	4192
Reflns collected/unique	37194/9332
R(int)	0.0312
Index ranges	-34 \leq h \leq 26, -22 \leq k \leq 22 -24 \leq l \leq 24
Refinement method	full-matrix, least-squares on F 2
FinalR indices	R1=0.0428, wR2=0.1472
[I \geq 2 σ (I)] a	R1=0.0543, wR2=0.1627
R indices (all data)	
GOF on F 2 (GOF) a	0.690

Table 2. Selected bond length (\AA) and bond angles (deg) for **2**

Zn(1)-O(2)	2.049(3)	Zn(2)-O(011)	2.356(3)
Zn(1)-O(2)	2.049(3)	Zn(2)-O(011)	2.356(3)
Zn(1)-N(2)	2.105(3)	Zn(2)-O(5)	2.444(4)
Zn(1)-N(1)	2.107(3)	O(2)-Zn(1)-O(1)	59.59(10)
Zn(1)-O(1)	2.312(3)	O(4)-Zn(1)-O(3)	59.68(12)
Zn(1)-O(3)	2.324(3)	N(2)-Zn(1)-N(1)	79.64(11)
Zn(2)-O(6)	1.994(3)	O(6)-Zn(2)-O(5)	58.07(13)
Zn(2)-O(014)	2.010(3)	O(014)-Zn(2)-O(011)	59.05(11)
Zn(2)-N(5)	2.097(3)	N(5)-Zn(2)-N(6)	79.01(12)

Table 3: Selected parameters for weak interactions in complex **2**

C(36)-H(36) \cdots O(3)	0.93	2.60	3.4620	155	-1/2+x, 1/2- y, -1/2+ z
C(37)-H(37) \cdots O(1)	0.93	2.43	3.1440	134	-1/2+x, 1/2- y, -1/2+ z
C(42)-H(42) \cdots O(3)	0.93	2.56	3.4090	152	1-x, y, 1/2- z

Fig. 1 shows the ORTEP diagram with atom numbering scheme of **2** while Fig. 2 shows $\pi \rightarrow \pi$ stacking interactions. The complex **2** exists as a neutral one-dimensional infinite zig-zag coordination chain. Each Zn(II) center is surrounded by two N donors from the 1,10-phenanthroline ring and four oxygen atoms from two carboxylate groups of two different azobenzene-4,4'-dicarboxylic acid molecules together in a distorted hexacoordinated geometry, as depicted in Fig. 1. The neighboring Zn (II) centers are connected by a azobenzene-4, 4'-dicarboxylate dianionic

moiety. The two azobenzene-4, 4'-dicarboxylate units are at 71.21° to one another and the two Zn (II) centers are separated at a distance of 17.35 \AA . The 1, 10-phenanthroline molecule acts as terminal ligand which prevents the chain growth in a straight forward direction; hence a zigzag chain is formed. The independent chains are linked through π - π interaction between the 1, 10-phenanthroline rings at a distance of 3.93 \AA . It results in the formation of channels (Fig. 2).

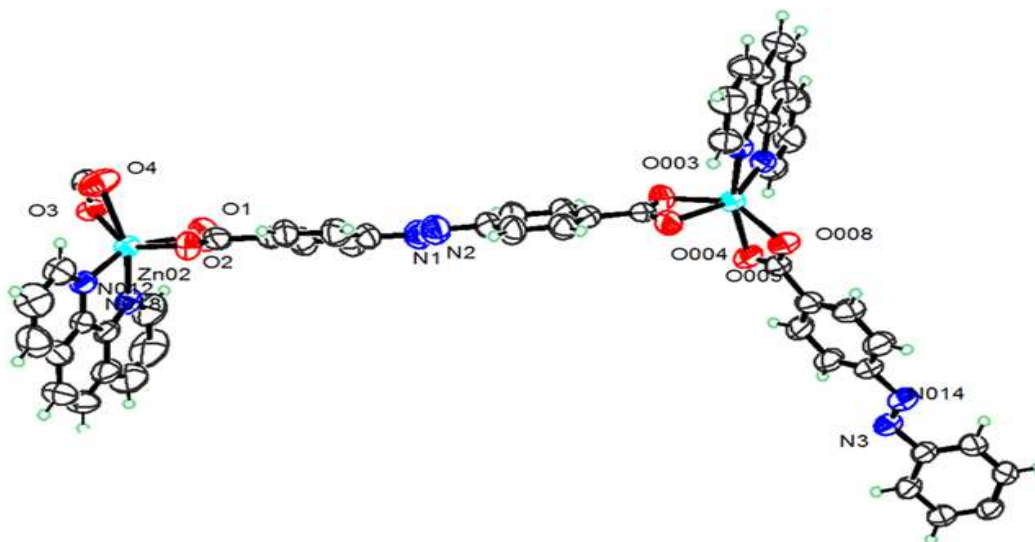


Fig. 2: Molecular structure (ORTEP) of compound **2**.

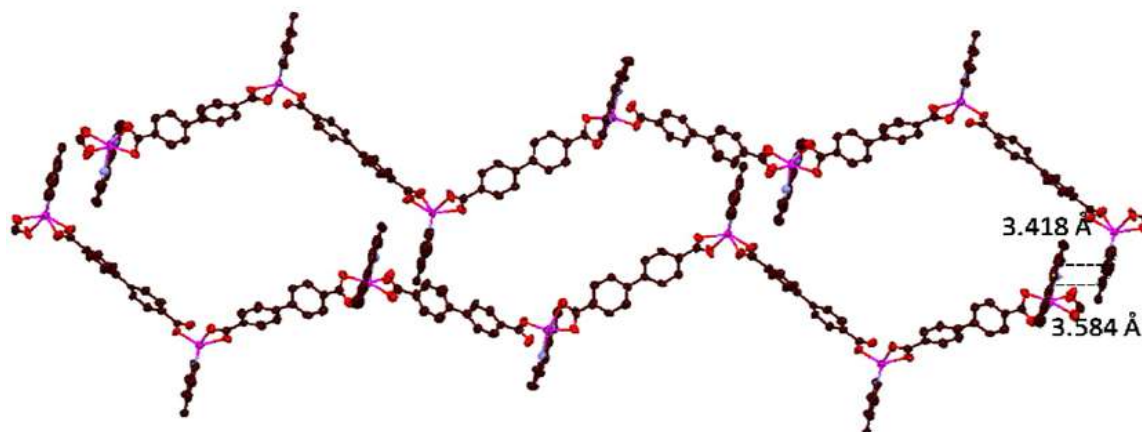


Fig. 3: Packing diagram of compound **2**. Dash lines indicate $\pi \rightarrow \pi$ stacking interactions.

Table 4: Performances of azo compounds as anode active materials in lithium-ion batteries

Active materials	Cycle performance	
	Capacity [mAhg^{-1}]	
	Discharge	Charge
Ligand 1	1392.4	278
MOF 2	1026.6	398.6

The electrochemical properties were evaluated by using the two azo-based materials **1** & **2** as anodes in Li-ion batteries. The MOF exhibited initial discharge and charge capacities of 1026.6 mA h g⁻¹ and 398.6 mA h g⁻¹ at a constant current density of 100 mA g⁻¹ respectively. For the pure ligand electrode, the discharge and charge capacities in the first cycle were 1392.4 mA h g⁻¹ and 278 mA h g⁻¹, respectively. The enhanced capacity of the MOF is possibly due to the redox reactions of both metal clusters and the ligand associated with lithiation/delithiation processes.

Conclusion

Both the azo compound **1** and MOF **2** electrodes exhibit good electrochemical performances with high specific capacities, good rate capabilities and cycling stabilities. The enhanced electrochemical performances of the MOF electrode may be mainly due to the fact that the large porosity of the two MOFs allows more lithium ion diffusion within their channels, the redox-active paddle-wheel metal clusters could provide multiple electrons, the $\pi \rightarrow \pi$ stacking improves electron conductivity and the open negatively charged O sites of the azo ligand help lithium storage. Thus the collective effect of porosity and redox reaction of the metal nodes and the organic ligand will strongly influence the electrochemical performances of MOF electrode.

Conflict of Interest

The authors declare that there is no conflict of interest with present publication.

Acknowledgement

The author is thankful to the members of dept. of chemistry, Tribhuvan University, T.R.M. Campus, Birgunj for their valuable suggestions and encouragement.

References

- Fu WF, Li HJ, Wang DH, Zhou LJ, Li L, Gan X, Xu QQ & Song HB (2009) A novel Kolbe reaction pathway for a selective one- and two-electron reduction of azo compounds. *Chem. Commun.* **37**: 5524-5526. DOI: [10.1039/b906910k](https://doi.org/10.1039/b906910k)
- Ghosh S, Usharani D, Paul A, De S, Jemmis ED & Bhattacharya S (2008) Design, Synthesis, and DNA Binding Properties of Photoisomerizable Azobenzene-Distamycin Conjugates: An Experimental and Computational Study. *Bioconjugate Chem.* **19**(12): 2332-2345. DOI: [10.1021/bc800130u](https://doi.org/10.1021/bc800130u)
- Guo X, Zhu G, Li Z, Sun F, Yang Z & Qiu S (2006) A lanthanide metal-organic framework with high thermal stability and available Lewis-acid metal sites. *Chemical communications* **30**: 3172-3174. DOI: [10.1039/B605428E](https://doi.org/10.1039/B605428E)
- Hu M, Pang X & Zhou Z (2013) Recent progress in high-voltage lithium-ion batteries. *J. Power Sources* **237**: 229-242. DOI: [10.1016/j.jpowsour.2013.03.024](https://doi.org/10.1016/j.jpowsour.2013.03.024)
- Li C, Hu X, Tong W, Yan W, Lou X, Shen M & Hu B (2017) Ultrathin Manganese-Based Metal-Organic Framework Nanosheets: Low-Cost and Energy-Dense Lithium Storage Anodes with the Coexistence of Metal and Ligand Redox Activities. *ACS Appl. Mater. Interfaces* **9**: 29829-29838. DOI: [10.1021/acsami.7b09363](https://doi.org/10.1021/acsami.7b09363)
- Luo C, Ji X, Hou S, Eidson N, Fan X, Liang Y, Deng T, Jiang J & Wang C (2018) Azo Compounds Derived from Electrochemical Reduction of Nitro Compounds for High Performance Li-Ion Batteries. *Adv. Mater* **30**(23): 1706498. DOI: [10.1002/adma.201706498](https://doi.org/10.1002/adma.201706498)
- Lyu Y, Wu X, Wang K, Feng Z, Cheng T, Liu Y, Wang M, Chen R, Xu L, Zhou J, Lu Y & Guo B (2021) An Overview on the Advances of LiCoO₂ Cathodes for Lithium-Ion Batteries. *Adv. Energy Mater* **11**(2): 2000982. DOI: [10.1002/aenm.202000982](https://doi.org/10.1002/aenm.202000982)
- Nishida S, Yamamoto Y, Takui T & Morita Y (2013) Organic Rechargeable Batteries with Tailored Voltage and Cycle Performance. *Chem Sus Chem* **6**: 794-797. DOI: [10.1002/cssc.201300010](https://doi.org/10.1002/cssc.201300010)
- Sheldrick GM (1990) Phase annealing in SHELX-90: direct methods for larger structures. *Acta Crystallogr A* **46**(6):467-473. DOI: [10.1107/S0108767390000277](https://doi.org/10.1107/S0108767390000277)
- Sheldrick GM (1997) SHELXS-97 Program for the Solution of Crystal Structures; University of Gottingen: Gottingen, Germany.
- Wu MK, Yi FY, Fang Y, Xiao XW, Wang SC, Pan LQ, Zhu SR, Tao K & L. Han (2017) An Ultrastable Metal-Organic Framework with Open Coordinated Sites Realizing Selective Separation toward Cationic Dyes in Aqueous Solution. *Cryst. Growth Des.* **17** (10) : 5458-5464. DOI: [10.1021/acs.cgd.7b00984](https://doi.org/10.1021/acs.cgd.7b00984)
- Yadav PK, Kumari N, Pachfule P, Banerjee R & Mishra L (2012) Metal [Zn(II), Cd(II)], 1,10-Phenanthroline Containing Coordination Polymers Constructed on the Skeleton of Polycarboxylates: Synthesis, Characterization, Microstructural, and CO₂ Gas Adsorption Studies. *Cryst. Growth Des.* **12**: 5311-5319. DOI: [10.1021/cg301277q](https://doi.org/10.1021/cg301277q)
- Yan R & Wang Q (2018) Redox-Targeting-Based Flow Batteries for Large-Scale Energy Storage. *Adv. Mater* **30**(47): 1802406. DOI: [10.1002/adma.201802406](https://doi.org/10.1002/adma.201802406)
- Zhou Y, Wu M, Luo Y, Pang B, Su X, Zhou M & Han L (2019) Redox active azo-based metal-organic frameworks as anode materials for lithium-ion batteries. *New J. Chem.* **43**: 1710-1715. DOI: [10.1039/C8NJ05014G](https://doi.org/10.1039/C8NJ05014G)